

On the nature of superconductivity in the anisotropic dichalcogenide NbSe₂{CoCp₂}_x

Ernst-Wilhelm Scheidt, Michael Herzinger, Andreas Fischer, D. Schmitz, J. Reiners, Franz Mayr, Florian Loder, M. Baenitz, Wolfgang Scherer

Angaben zur Veröffentlichung / Publication details:

Scheidt, Ernst-Wilhelm, Michael Herzinger, Andreas Fischer, D. Schmitz, J. Reiners, Franz Mayr, Florian Loder, M. Baenitz, and Wolfgang Scherer. 2015. "On the nature of superconductivity in the anisotropic dichalcogenide NbSe₂{CoCp₂}_x." Journal of Physics: Condensed Matter 27 (15): 155701. <https://doi.org/10.1088/0953-8984/27/15/155701>.

On the nature of superconductivity in the anisotropic dichalcogenide $\text{NbSe}_2\{\text{CoCp}_2\}_x$

E-W Scheidt¹, M Herzinger¹, A Fischer¹, D Schmitz¹, J Reiners¹, F Mayr², F Loder³, M Baenitz⁴ and W Scherer¹

¹ CPM, Institut für Physik, Universität Augsburg, 86135 Augsburg, Germany

² EPV, EKM, Institut für Physik, Universität Augsburg, 86135 Augsburg, Germany

³ EPVI, EKM, Institut für Physik, Universität Augsburg, 86135 Augsburg, Germany

⁴ Max-Planck-Institut für Chemische Physik fester Stoffe, 01187 Dresden, Germany

E-mail: Wolfgang.Scherer@physik.uni-augsburg.de

Abstract

We present a detailed study of the superconducting properties of the weakly pinned, quasi-two-dimensional superconductor 2H-NbSe₂, and its intercalated variant NbSe₂{CoCp₂}_{0.26}. The intercalation of 2H-NbSe₂ with the organometallic donor molecule cobaltocene (CoCp₂) hardly affects the superconducting properties within the layers. However, the properties perpendicular to the layers change significantly due to the large expansion of the layer spacings of the host lattice in the *c*-direction by a factor of about two. In particular, the superconducting anisotropy factor Γ increases from 3.3 in the parent compound 2H-NbSe₂ up to 4.4 in the intercalated species. Therefore, NbSe₂{CoCp₂}_{0.26} is an excellent candidate to analyze how the anisotropy effects the superconducting mechanism in layered dichalcogenides, and to evaluate the various models proposed in the literature to account for the anisotropy in 2H-NbSe₂. While a two-gap model and an anisotropic single-gap model are competing concepts to describe the almost linear T^2 -dependence of $\Delta C/T$ in low-dimensional dichalcogenides, our comparative study suggests that a single-gap model with an anisotropic Fermi-surface is sufficient to capture the $\Delta C/T(T)$ behavior in our samples qualitatively.

Keywords: low-dimensionality, superconductors, BCS-theory, dichalcogenide

(Some figures may appear in colour only in the online journal)

1. Introduction

Among the numerous studies dealing with the incidence and nature of superconductivity, low-dimensional materials play an increasingly important role as benchmark and model systems [1]. The reason for this is closely connected with the discovery of novel quasi-one or two-dimensional superconductors, such as the rare-earth transition metal carbide Sc₃CoC₄ [2, 3], or the boride MgB₂ and the intercalated, iron-based selenides Li_{*x*}Fe₂Se₂(NH₃)_{*y*} [4, 5], respectively. Here we report on superconductivity in the new highly anisotropic layered dichalcogenide NbSe₂{CoCp₂}_{0.26}, where cobaltocene (CoCp₂ = (C₅H₅)₂Co) represents an intercalated electronic donor molecule.

Quasi-two-dimensional (2D) intercalation compounds of transition metal dichalcogenide superconductors are typically characterized by highly pronounced anisotropic electronic properties [1]. Despite extensive studies, the superconducting mechanism of this class of compounds is still poorly understood. Among these compounds, 2H-NbSe₂ represents perhaps the most prominent low-dimensional material studied during the past fifty years [6]. After the discovery of the high temperature superconductor MgB₂ [4], a benchmark system for multi-band superconductivity [7], 2H-NbSe₂ experienced a renaissance of research activities [8]. In particular, it represents a well-suited candidate for probing the multi-band model in a 2D superconductor, due to the negligible extent of vortex pinning. Furthermore, the critical temperature of

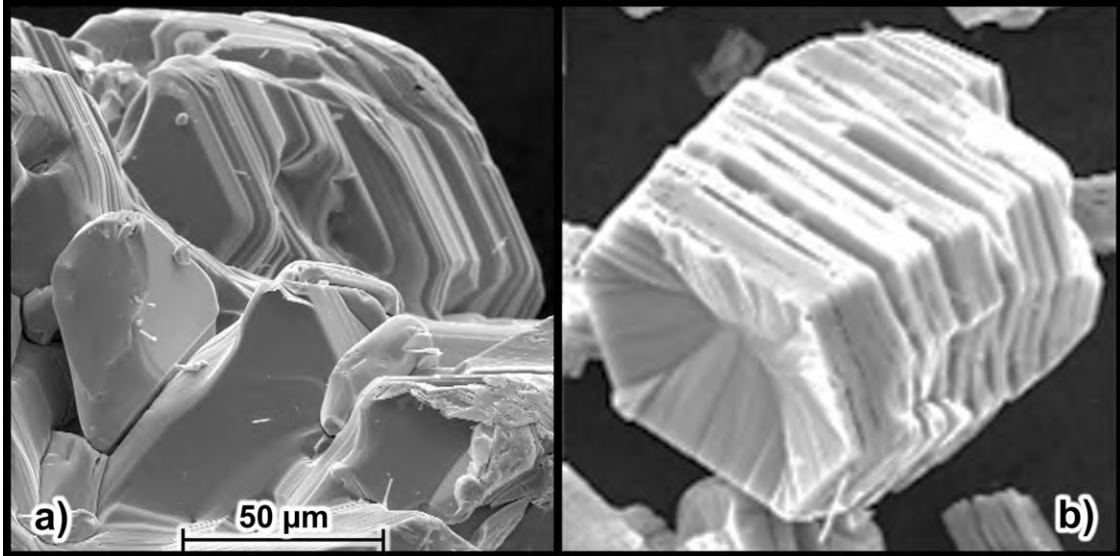


Figure 1. ESEM-micrograph of (a) 2H-NbSe₂ and (b) NbSe₂{CoCp₂}_{0.26} crystals reflecting the layered structure of these materials.

$T_c = 7.2$ K is the highest temperature reported hitherto for dichalcogenid systems [9]. Besides this, 2H-NbSe₂ shows a re-entrant peak effect, as evidenced by resistivity and AC-susceptibility measurements [10]. An additional feature is the presence of a charge density wave (CDW) transition at the Peierls-temperature $T_{CDW} = 33$ K [11]. The reason for the origin and emergence of such a CDW in NbSe₂ remains up to now an unresolved question [12].

In order to enhance the anisotropic character we designed the geometrical and electronic structure of 2H-NbSe₂ via the intercalation of high quality 2H-NbSe₂ single crystals with the organometallic donor molecule cobaltocene (CoCp₂), which also acts as a spacer molecule causing almost a doubling of the layer spacings in the c -direction upon intercalation. While the intercalation by electronically inert organic guest molecules is reported to reduce the superconducting transition temperature T_c from 7.2 K in 2H-NbSe₂ to temperatures below $T_c < 3$ K [9], an opposite behavior is observed in NbSe₂{CoCp₂}_{0.26} upon intercalation with the electronic donor molecule cobaltocene. T_c is slightly raised with respect to the original host lattice to $T_c^{onset} = 7.5$ K. Furthermore, susceptibility, specific heat, and resistivity studies (parallel and perpendicular to the 2H-NbSe₂-layers) of NbSe₂{CoCp₂}_{0.26} reveal unusual pinning properties as well as a non-BCS-like linear T^2 -dependence of $\Delta C/T$ sequences. A re-entrant peak effect, known from the host species 2H-NbSe₂ [10], is also observed. Therefore, NbSe₂{CoCp₂}_{0.26} may be a good candidate for a comparative study to distinguish between different anisotropic superconducting models, like the two-gap model [8] or the anisotropic single-gap model [13].

2. Sample preparation and characterisation

2H-NbSe₂ single crystals have been synthesized via chemical transport in sealed quartz-ampoules (length: 150 mm; inner diameter: 10 mm) with iodine as a transport agent in a tube-furnace. The transport reaction was carried out using a

temperature gradient: source ($T_1 = 840$ °C) and sink ($T_2 = 600$ °C). Plate-like NbSe₂ single crystals were isolated and intercalated with cobaltocene (CoCp₂) in acetonitrile (CH₃CN) at a temperature of 65 °C under inert gas conditions (Ar) for four weeks and characterized by ESEM micrographs, ICP-OES (Ionic Coupled Plasma-Optical Emission Spectroscopy), x-ray powder diffraction, and physical property measurements. The sample stoichiometry of one part of the same batch was determined via ICP-OES as NbSe₂{CoCp₂}_{0.26} [14].

Figures 1(a) and (b) show an ESEM-micrograph of the crystalline host material 2H-NbSe₂ and of the intercalated NbSe₂{CoCp₂}_{0.26} sample at the same magnification, respectively. Both images show the hexagonal shape of native and intercalated 2H-NbSe₂ crystals. The partial exfoliation of the NbSe₂ lattice as a direct consequence of the intercalation process is clearly visible and documents the successful filling of the van der Waals gaps inbetween the individual (NbSe₂)-layers. A subsequent x-ray powder analysis reveals a stage-one-type intercalation variant since all the interlayer gaps in 2H-NbSe₂ are at least partially filled.

In figure 2 the powder diffraction pattern of 2H-NbSe₂ is plotted. A strong preferred orientation of the powder samples was observed due to the pronounced two-dimensional shape of the 2H-NbSe₂ crystals. In order to determine precise lattice parameters for the host as well as the intercalated lattice, a Le Bail profile fitting as implemented in the Jana2006 program [15] has been used. The lattice constants of 2H-NbSe₂, which crystallizes in the hexagonal space group $P6_3/mmc$, have been determined to $a = 0.344\,570(7)$ nm and $c = 1.255\,00(4)$ nm. The sharp Bragg-peaks and the absence of additional reflections are in line with the high crystal-quality and purity of the sample. Upon intercalation, the 00ℓ -series of the host lattice (the blue curve in figure 2) shifts to lower diffraction angles (the green curve in figure 2) in agreement with the expected expansion of the inter-layer spacing, yielding a new c -axis parameter of $2.3697(1)$ nm, whereas the a -axis expands only slightly to $a = 0.346\,460(7)$ nm. Since each unit

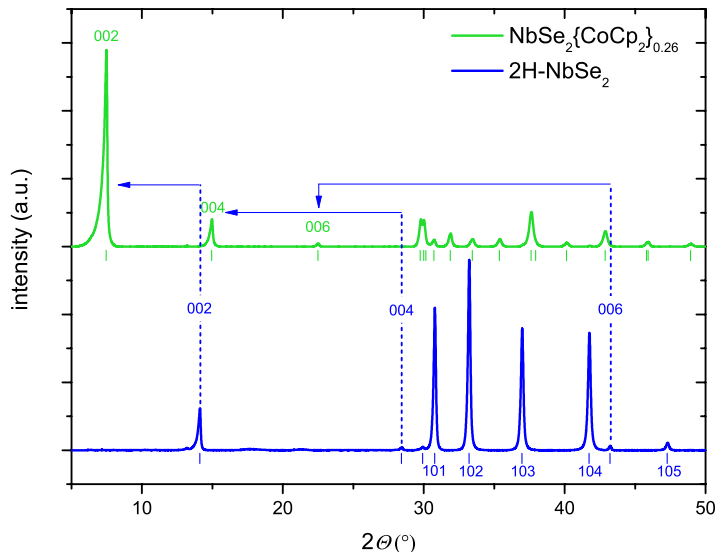


Figure 2. Comparative powder x -ray diffraction studies of the 2H-NbSe₂ (blue, bottom) and the intercalated species 2H-NbSe₂{CoCp₂}_{0.26} (green, top). The vertical lines below the patterns indicate the refined peak positions according to the space group $P6_3/mmc$ of 2H-NbSe₂ and its intercalated species.

cell contains two NbSe₂-layers (with the Nb-atoms located at $z = 0.25$ and $z = 0.75$, where z is the fractional atomic coordinate along the c -axis), the layer expansion corresponds to $\Delta c/2 = 0.5574$ nm. This is in good agreement with the value published by Dines *et al* for the layer expansion upon CoCp₂ intercalation ($\Delta c = 0.556$ nm [16]). We note that the Bragg-intensities from the host lattice vanished completely. This suggests that the intercalation process was complete (the green curve in figure 2) in line with an intercalation degree of 0.26, which is close to the theoretical limit of $x = 0.336$ in related dichalcogenides such as SnSe₂ [17].

A further indicator for the high quality of the samples is the residual resistivity ratio (RRR). In the case of 2H-NbSe₂ the RRR is determined to be 37 between 7.5 K and 300 K. This value is higher than most of the values discussed in the literature [18–21]. For the intercalated sample the RRR = 33 is slightly reduced indicating—if at all—a marginal loss of the crystallinity.

3. Experimental details

The diffraction patterns depicted in figure 2 were measured in transmission mode on a HUBER Guinier diffractometer equipped with a Mo-K_{α1}-source (2H-NbSe₂), or alternatively with a Cu-K_{α1}-source (NbSe₂{CoCp₂}_{0.26}) and a HUBER G670 Guinier camera. The background intensity was removed using the DIFFRACplus EVA software (Bruker AXS, Germany). For better comparison in figure 2, the $2\theta_{Mo}$ axis for the pattern of 2H-NbSe₂ has been rescaled to Cu-K_{α1} radiation.

The DC magnetic susceptibility measurements were performed between 2 K and 300 K in an applied magnetic field of up to 5 T using a commercial SQUID magnetometer (MPMS-7) from Quantum Design. To align the single crystals parallel and perpendicular to the magnetic fields, small single crystalline plates (≤ 4 mm \times 2.5 mm edge lengths) were embedded in NaCl powder (5N; Alfa Aesar) and confined

by two quartz glass rods inside a straw to prevent sample reorientation during the measurement. The accuracy of the individual crystal orientation with respect to the field is estimated to be better than $\pm 5^\circ$. For the AC susceptibility we used a SQUID Magnetometer (MPMS-5) with an AC-option, and for magnetic fields up to 14 T a state of the art SQUID-VSM system from Quantum Design was utilized. The specific heat experiments were performed with a commercial physical property measurement system (PPMS) equipment between 2 K and 300 K in magnetic fields up to 5 T. For the electrical transport measurements we performed a four probe method using the PPMS. To avoid Lorentz currents, the external magnetic field and the current flow were applied in the same direction parallel to the layers. The dimensions of the single crystal employed for the resistivity measurements were 3.4 mm \times 0.6 mm (thickness $d \approx 150$ μ m), and the distance between the current and voltage contacts (size ≈ 0.6 mm \times 0.4 mm) was ≈ 2.4 mm and 0.7 mm, respectively.

4. Experimental results and discussion

4.1. Susceptibility

The temperature dependent magnetic dc-susceptibility ($\chi_V(T)$) of NbSe₂{CoCp₂}_{0.26} is depicted in figure 3 for zero field cooled (ZFC) and field cooled (FC) cycles in a low magnetic field applied perpendicular and parallel to the ab -planes. For the ZFC sequence the sample was first cooled down to 2 K in a zero field, where the earth magnetic field was compensated within an error bar of 1 μ T by the so-called *TinyBee* setup described in detail in [22]. In the subsequent heating run a small magnetic field of $\mu_0 H = 0.5$ mT was applied to record the susceptibility data up to 8 K. For the susceptibility measurements with H perpendicular to the ab -plane ($H \perp ab$) a demagnetization factor of $N = 0.8$ was taken into account. This factor is estimated experimentally by measuring a lead

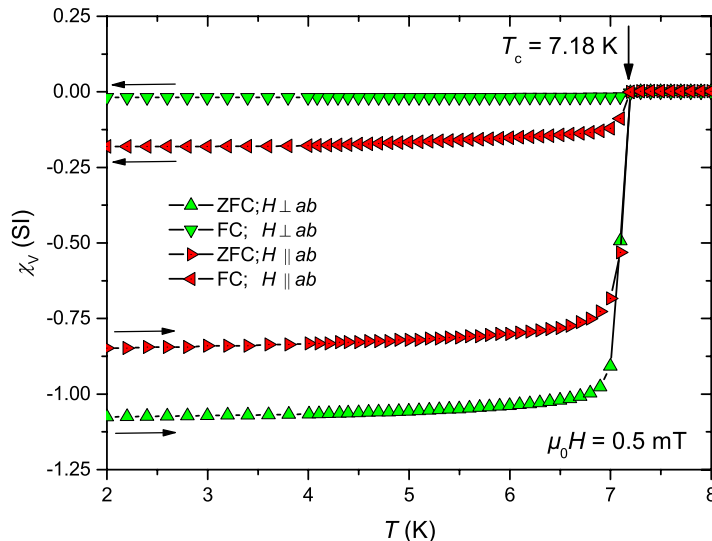


Figure 3. ZFC and FC volume susceptibility (χ_V) of $\text{NbSe}_2\{\text{CoCp}_2\}_{0.26}$ with μ_0H perpendicular and parallel to the ab -planes. For the measurement with $H \perp ab$ a demagnetization factor of $N = 0.8$ was considered.

plate with a shape nearly identical to the investigated sample ($\approx 4 \text{ mm} \times 2.5 \text{ mm}$; slight trapezoid). For the volume susceptibility χ_V we calculated the density of $\text{NbSe}_2\{\text{CoCp}_2\}_{0.26}$ from the lattice parameters and the stoichiometry of the sample known from the ICP-OES and elementary analysis, resulting in a value of $\rho = 4.052 \text{ g cm}^{-3}$.

In figure 3 all $\chi_V(T)$ curves exhibit a sharp superconducting transition at $T_c = 7.18 \text{ K}$ for the ZFC and FC procedures. This critical temperature is virtually identical to the one of the host substance and is slightly smaller than $T_c^{\text{onset}} = 7.5 \text{ K}$ estimated from our resistivity studies (section 4.3, figure 7(a)). This result is remarkable due to the fact that previous intercalations of 2H-NbSe_2 with electronically innocent guest molecules yielded a significant reduction of T_c and values between 0.6 K and 6.88 K [9, 19, 21, 23, 24].

Furthermore, the $\chi_V(T)$ -data of $\text{NbSe}_2\{\text{CoCp}_2\}_{0.26}$ show some deviation from an ideal bulk superconducting behavior. In the ideal case, the ZFC procedure in low magnetic fields results in a complete shielding state of the sample with $\chi_V = -1$ at low temperatures. The FC measurement provides information about the strength of the flux expulsion due to the Meissner effect. In the case of hard type-II superconductors, such as the high temperature superconductor YBaCuO [25], a superconducting volume susceptibility in the range of $-1 \leq \chi_V \leq -0.5$ is usually expected, in contrast to our findings for $\text{NbSe}_2\{\text{CoCp}_2\}_{0.26}$ with $\chi_V \approx -0.05$ ($H \perp ab$).

For $\text{NbSe}_2\{\text{CoCp}_2\}_{0.26}$ we observed in the case of $H \parallel ab$ that the ZFC procedure results in a partial screening ($\chi_V > -1$), mainly due to the presence of a normal state region in the van der Waals gap between the $(\text{NbSe}_2)_2$ layers. On the other hand for $H \perp ab$ a full screening is expected. The deviation of 7% from the ideal value may be due to the error in the determination of the demagnetization factor or the sample density. For the FC measurement with $H \parallel ab$ the sample is exposed to a maximal field of $\mu_0H = 0.5 \text{ mT}$ due to the vanishing demagnetization factor. This leads to a flux expulsion in the superconducting planes but not in the

inter-layer space. Therefore, the resulting intermediate phase gives rise to a small but not negligible Meissner-phase. On the contrary, for $H \perp ab$ the demagnetization factor is close to one, due to the plate-like shape of the sample. This may lead to local magnetic fields higher than $\mu_0H_{c1\perp}$, resulting in flux-penetration with vortex field strengths higher than $\mu_0H_{c1\perp}$. As a result, the Meissner effect may be superimposed by this flux pinning process and therefore only a negligible Meissner effect is observed.

This deviation from an ideal superconducting behavior strongly points to a pronounced anisotropic superconductor with a layered structure of superconducting planes which are weakly coupled by van der Waals forces.

4.2. Critical magnetic fields and Ginzburg–Landau parameters

In order to calculate the microscopic superconducting parameters like the London penetration depth (λ), the GL coherence length (ξ), and the GL parameter (κ), the lower and upper critical fields perpendicular and parallel to the ab -planes are determined from magnetization curves and from temperature dependent specific heat and resistivity measurements in various magnetic fields.

The lower critical fields of 2H-NbSe_2 and $\text{NbSe}_2\{\text{CoCp}_2\}_{0.26}$ are estimated from magnetization measurements $\mu(\mu_0H)$ at very low magnetic fields, using the high resolution of $\mu_0\Delta H = 1 \mu\text{T}$ increments accomplished by the *TinyBee* setup [22]. In figure 4(a) the magnetic moment versus magnetic field for 2H-NbSe_2 in the case of H perpendicular to the ab -planes at 2 K is plotted in the range between 0 and 4 mT using minute increments of $\mu_0\Delta H = 0.025 \text{ mT}$. The linear fit (employing $\mu(H)$ data below 0.5 mT) shows the first deviation from the magnetization curve at approximately 1 mT . According to a common procedure in the literature (see, e.g. [26]) the latter value can therefore be employed to specify μ_0H_{c1} at 2 K . This is in accordance with the kink in the

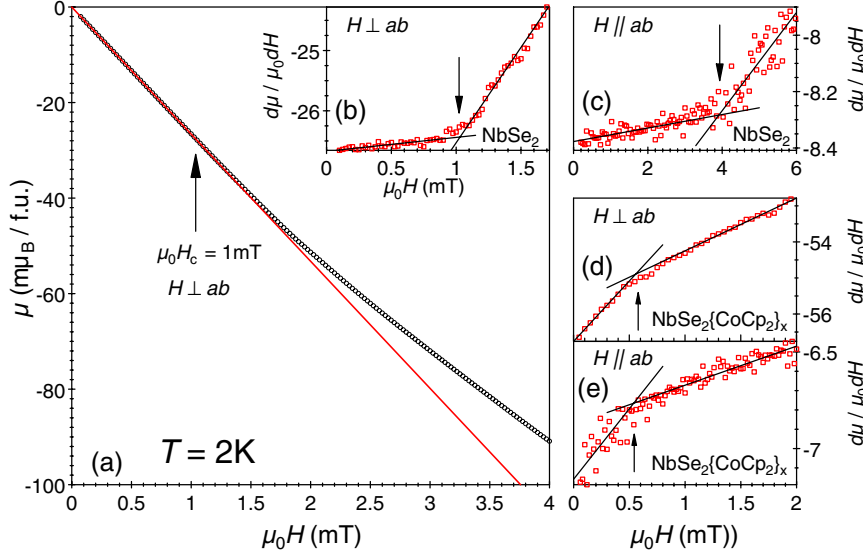


Figure 4. (a) The initial magnetization curve $\mu(\mu_0 H)$ up to 4 mT of NbSe₂ with H perpendicular to the ab -planes at $T = 2$ K. The red line is a linear fit to the magnetization data below 0.5 mT. In the insert (b) the first derivative of the magnetic moment μ with respect to the magnetic field $\mu_0 H$ is plotted versus $\mu_0 H$ in the range between 0 and 1.7 mT. The solid lines are linear fits to the data. The point of intersection defines $\mu_0 H_{c1}$. Such a plot is also shown in (c) for NbSe₂ with H parallel to the ab -planes and in (d) and (e) for NbSe₂{CoCp₂}_x ($x = 0.26$) with H perpendicular and parallel to the ab -planes, respectively.

derivative $\frac{d\mu}{\mu_0 dH}$, as shown in figure 4(b). This kink in the derivative $\frac{d\mu}{\mu_0 dH}$ is, however, a more stringent criterion for the determination of $\mu_0 H_{c1}$, because its location is less dependent on the choice and size of the fitting range and was therefore used to extract the H_{c1} values. This assessment is a sensitive indicator to identify the magnetic field $\mu_0 H_{c1}$, which is defined as the field where the first flux in the form of a quantized vortex penetrates the sample and starts to increase continuously with an increasing magnetic field [1]. It should be mentioned that for NbSe₂, $\frac{d\mu}{\mu_0 dH}(\mu_0 H)$ shows a slight increase for small fields in both field orientations, which may be due to a small flux penetration caused by sample inhomogeneities, thereupon the magnetic flux penetrates the sample in the form of quantized vortices visible by a pronounced increase in the derivative $\frac{d\mu}{\mu_0 dH}$, as shown in figures 4(b) and (c).

In contrast to this, figures 4(d) and (e) show for the intercalated sample NbSe₂{CoCp₂}_{0.26} a strong initial flux penetration. At a distinct magnetic field the slope of the derivative $\frac{d\mu}{\mu_0 dH}$ changes to smaller values indicating a reduced rate of flux penetration. This unusual behavior hints at unquantized flux penetration in the intercalated 2H-NbSe₂ already below H_{c1} . This observation is likely explained by the large spacial separation of the superconducting layers. In the case of magnetic fields above H_{c1} , the screening currents become sufficiently large to channel the flux into quantized vortices. Since the spacial extent of a vortex, given by the penetration depth λ , is far larger than the layer distance in 2H-NbSe₂, the vortex penetration rate above H_{c1} remains essentially unaffected by the subtle and additional increase in the inter-layer distance due to the intercalation of the cobaltocene molecules.

The lower critical field $\mu_0 H_{c1}$ at zero temperature is determined by extrapolating the magnetic field data at 2 K and

T_c , using the empiric parabolic relation [27]

$$\mu_0 H_{c1}(T) = \mu_0 H_{c1}(0) \times [1 - (T/T_c)^2] \quad (1)$$

by taking into account a demagnetization factor of $N = 0.8$ for the applied field H perpendicular to the ab -planes. The resulting lower critical field values with H parallel and perpendicular to the ab -planes are depicted in figures 4(b)–(e) and are summarized in table 1 for NbSe₂ and NbSe₂{CoCp₂}_{0.26}, respectively.

The upper critical fields H_{c2} perpendicular and parallel to the ab -planes are extracted from specific heat and resistivity measurements, respectively (for details see below). For NbSe₂{CoCp₂}_{0.26}, the electronic contribution to the specific heat divided by temperature $\Delta C/T$ is plotted for H perpendicular to the ab -planes versus T^2 in various magnetic fields up to 5 T in figure 5(a). The critical temperature is suppressed gradually by the magnetic field from $T_c = 7.12$ K to a temperature below 2 K for $\mu_0 H > 5$ T. The specific heat discontinuity at $T_c(0)$ of $\delta C/T \simeq 31.6$ mJ mol⁻¹ K² divided by the Sommerfeld coefficient in the normal state $\gamma \simeq 22.1$ mJ mol⁻¹ K² yields the thermodynamic ratio $\delta C/\gamma T_c = 1.43$, which surprisingly matches the expected value of 1.43 for a weakly coupled BCS superconductor [28]. In contrast to this, a somewhat higher $\delta C/\gamma T_c$ ratio is observed in the parent compound 2H-NbSe₂ with varying values between 1.96 and 2.12, which may be connected to a more pronounced electron-phonon coupling (see table 1 and [29, 30]). Such enhanced values are generally known for layered superconductors, e.g. FeSe ($\delta C/\gamma T_c = 1.65$) [31].

Furthermore, it should be mentioned that the nearly linear trend in the $\Delta C/T$ versus T^2 plot below T_c of NbSe₂{CoCp₂}_{0.26} (figure 5(a)) is also observed in the parent species [13, 29, 30]. This linearity is unusual for single band s -wave superconductors. A similar superconducting behavior

Table 1. Overview of the superconducting parameters of 2H-NbSe₂ and the intercalated species NbSe₂{CoCp₂}_{0.26} from this work, in comparison with selected studies from the literature [8, 40–42].

	2H-NbSe ₂ [40]	2H-NbSe ₂ [41]	2H-NbSe ₂ [42]	2H-NbSe ₂ [8]	2H-NbSe ₂ this work	NbSe ₂ {CoCp ₂ } _{0.26} this work
T_c	7.38 K	7.07 K	7.15 K	7.15 K	7.15 K	7.35 K
$\mu_0 H_{c2\parallel}$		12.5 T	17.3 T	12.3 T	14.1 T	18.5 T
$\mu_0 H_{c2\perp}$	4.3 T*	3.65 T	5.3 T	4.1 T	4.3 T	4.2 T
$\mu_0 H_{c1\parallel}$				3.9 mT	4.24 mT	0.58 mT
$\mu_0 H_{c1\perp}$				9 mT	5.49 mT	3.13 mT
λ_{\parallel}	69 nm			265 nm	330 nm	455 nm
λ_{\perp}	230 nm			797 nm	524 nm	3561 nm
ξ_{\parallel}	7.7 nm	9.5 nm	7.88 nm	9 nm	8.75 nm	8.86 nm
ξ_{\perp}	2.3 nm	2.8 nm	2.42 nm	3 nm	2.67 nm	2.02 nm
κ_{\parallel}	30	72	29	86	86	300
κ_{\perp}	9	21	11	30	38	51
$\delta C/\gamma T_c$	1.97 [13]	1.96	2.14	2.12 [29]	2.05	1.43

Note: The symbols \parallel and \perp refer to directions parallel and perpendicular to the ab plane, respectively. The * marks the upper critical fields $B_{c2\perp}$, which is estimated from figure 2 in [40].

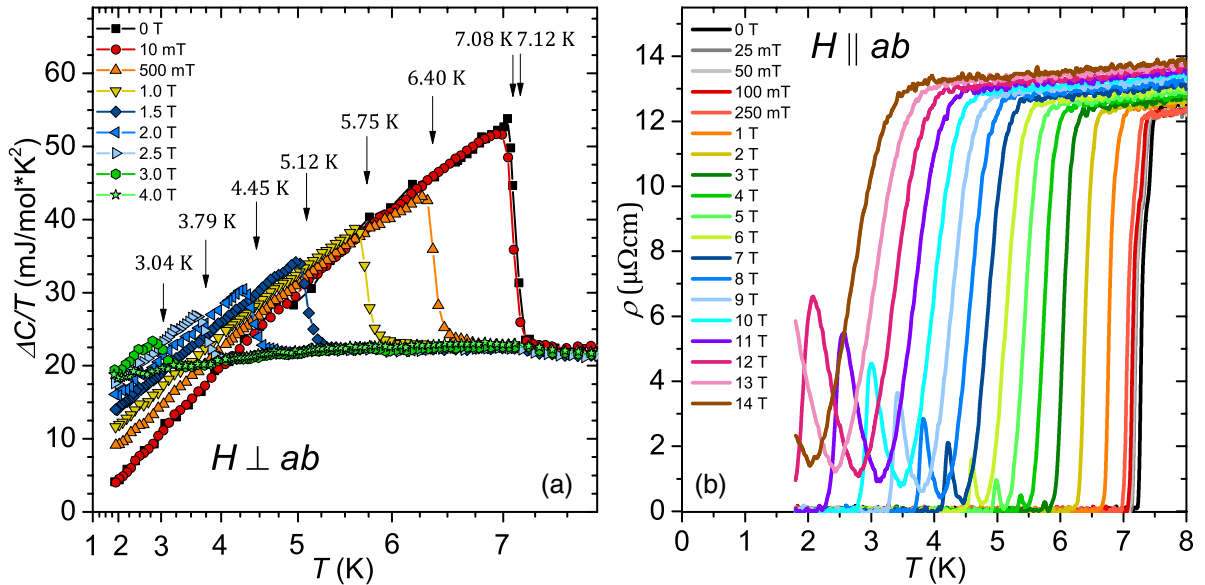


Figure 5. (a) Temperature-dependent electronic contribution of the specific heat plotted as $\Delta C/T$ versus T^2 of NbSe₂{CoCp₂}_{0.26} for various magnetic fields (as labeled) perpendicular to the ab -planes. (b) Temperature-dependent electrical resistivity for various magnetic fields (as labeled) parallel to the ab -planes.

is also found in the intermetallic compound MgB₂, which is discussed with respect to a second superconducting band at the Fermi level [32]. In particular, for the host sample 2H-NbSe₂, Huang *et al* proposed that a two-gap scenario is more favorable than an anisotropic s -wave model [29]. We will outline in the following that the latter proposal is not supported by our own study. We give a more detailed discussion and comparison to the model calculations in section 5.

For NbSe₂{CoCp₂}_{0.26} the temperature dependency of the in-plane resistivity in various magnetic fields is shown in figure 5(b) in the temperature range between 1.8 K and 8 K. Towards lower temperatures, after the initial steep drop of the resistivity due to the onset of superconductivity, the sample shows a finite resistivity, which again vanishes on further cooling. This observed reentrant behavior is also known from the host sample 2H-NbSe₂ [33]. The out-of-plane resistivity

behavior could, however, not be determined, although a special set-up was used as described in [34].

In figure 6 the phase diagrams of the upper (a) and lower (b) critical magnetic fields parallel and perpendicular to the ab -planes are presented. For $\mu_0 H_{c2\parallel}$ the critical temperatures are obtained from the 50% values of the normal state resistivity (figure 5(b)) slightly below the onset of superconductivity. For $H_{c2\perp}$ the T_c data are determined at that temperature, where the specific heat discontinuity of the superconducting anomaly reaches half of the values $\delta C/T$ (figure 5(a)). For both branches ($H\parallel ab$ and $H\perp ab$ in figure 6(a)) we extrapolate the $\mu_0 H_{c2}$ values in the linear region between 2 and 6 K down to zero temperature taking into account the WHH-theory [35]. It should be mentioned that a positive curvature of $\mu_0 H_{c2\parallel}(T)$ is observed just below T_c , which is not in line with the WHH-theory. However, this feature appears to be a characteristic

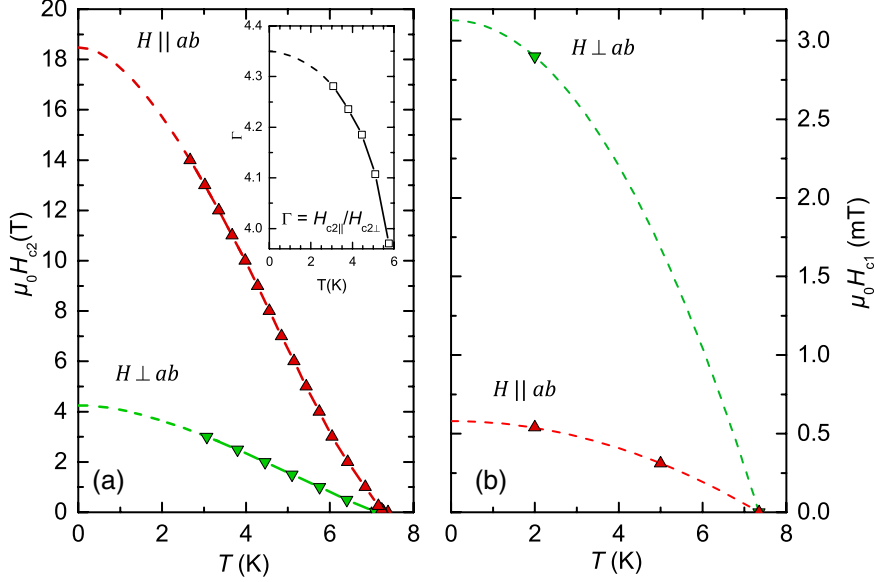


Figure 6. (a) Temperature dependence of the upper critical magnetic field, $\mu_0 H_{c2}$, and (b) of the lower critical field, $\mu_0 H_{c1}$, perpendicular and parallel to the NbSe₂ planes of NbSe₂{CoCp₂}_{0.26}. The insert displays the temperature dependent anisotropy factor Γ . The solid lines are guides for the eyes. The dashed lines are fits to the data according to the WHH-theory [35] for $\mu_0 H_{c2}(T)$ and to the empiric relation (see equation (1)) for $\mu_0 H_{c1}(T)$, respectively.

$H_{c2||}(T)$ signature observed in many layered superconductors (see chapter 6 in [1]), and in particular also in the host substance 2H-NbSe₂ [8]. This positive, upward curvature may be due to the onset of a dimensional cross-over [36], or caused by an anisotropic Fermi-surface [20]. The phase boundaries of the lower critical fields down to zero temperatures are generated from the values of the lower critical fields at 2 K (see figures 4(d) and (e)), 5 K and from the T_c values at $H = 0$, using the empiric relation for $\mu_0 H_{c1}(T)$ (see equation (1)). The resulting lower and upper critical field values at $T = 0$ K are tabulated in table 1, in comparison with selected results of the host sample 2H-NbSe₂.

The upper critical field ratio $H_{c2||}/H_{c2\perp}$ of NbSe₂{CoCp₂}_{0.26} defines the anisotropy factor Γ , which is about 4.4 at $T = 0$. This value is 34% larger than that of 2H-NbSe₂ and is similar to those values found in different single crystalline MgB₂ samples (for an overview see [37]). For both species, NbSe₂ and MgB₂, a multi-band scenario is discussed in the literature, which goes along with a temperature dependent anisotropy factor $\Gamma(T)$ [8, 37]. Such behavior is also observed in NbSe₂{CoCp₂}_{0.26} (insert of figure 6(a)), but the change of the anisotropy per Kelvin $\frac{d\Gamma}{dT}$ of approximately 0.075 K⁽⁻¹⁾ is two times smaller than in MgB₂—the benchmark system for multi-band superconduction. This may be due to different determination methods of $\Gamma(T)$ [8, 37, 38]. Even though the change of $\Gamma(T)$ is smaller in comparison to MgB₂, this criterion does not disqualify NbSe₂{CoCp₂}_{0.26} as suitable candidate for a multi-band scenario at this stage of our analysis.

For a detailed comparison between 2H-NbSe₂ and NbSe₂{CoCp₂}_{0.26} we also calculated the microscopic superconducting parameters ξ , λ , and κ directly from the critical magnetic fields according to the anisotropic GL theory [1]. Here the GL coherence length ξ_{GL} is extracted

from the upper critical field using the following equations:

$$\mu_0 H_{c2||} = \frac{\Phi_0}{2\pi \xi_{||} \xi_{\perp}} \quad \text{and} \quad \mu_0 H_{c2\perp} = \frac{\Phi_0}{2\pi \xi_{||}^2} \quad (2)$$

with the flux quantum $\Phi_0 = h/2e$. The London penetration depth λ is extracted from the lower critical field:

$$\mu_0 H_{c1||} = \frac{\Phi_0}{4\pi \lambda_{||} \lambda_{\perp}} \times \ln \kappa_{||} \quad \text{and} \quad \mu_0 H_{c1\perp} = \frac{\Phi_0}{4\pi \lambda_{||}^2} \times \ln \kappa_{\perp} \quad (3)$$

with the GL-parameters

$$\kappa_{||} = \left(\frac{\lambda_{||} \lambda_{\perp}}{\xi_{||} \xi_{\perp}} \right)^{1/2} \quad \text{and} \quad \kappa_{\perp} = \frac{\lambda_{||}}{\xi_{||}} \quad (4)$$

which are extracted from microscopic superconducting parameters.

All the quantities are presented in table 1 together with those of selected studies in order to compare our results of the host species 2H-NbSe₂ with former findings in the literature (see, [8, 40–42]). First of all it should be mentioned that within the variation of different calculations and measurement procedures, the superconducting quantities like ξ , λ , and κ of the parent compound 2H-NbSe₂ are in good agreement with previous results. The direct comparison between the host species and NbSe₂{CoCp₂}_{0.26} surprisingly reveals that the microscopic superconducting GL quantities, $\xi_{||}$ and $\lambda_{||}$, remain almost unchanged within the layers upon CoCp₂ intercalation. On the contrary, the coherence length perpendicular to the layers ξ_{\perp} diminishes by 25% after CoCp₂ intercalation, and is of the order of the inter-layer distance of the intercalated species. In addition, the penetration depth parallel to the layers $\lambda_{||}$ is approximately of the same order of magnitude for both species, whereas for λ_{\perp} a drastic increase by a factor of

4.5 is observed between the host and the intercalated sample, respectively.

This analysis emphasizes the outstanding character of the intercalated samples, as the superconducting properties within the layers remain almost unchanged but change significantly perpendicular to the layer along the c lattice parameter. This is a surprising result since cobaltocene (CoCp_2) is an electronic donor molecule, which is capable of transferring its unpaired electron into the conduction band of suitable host materials which might act as electron acceptors. Indeed, the electron transfer is indicated by an enhancement of the Sommerfeld coefficient γ in the intercalated sample (NbSe_2 : $\gamma = 18 \text{ mJ mol}^{-1} \cdot \text{K}^{-2}$; $\text{NbSe}_2\{\text{CoCp}_2\}_{0.26}$: $\gamma = 22 \text{ mJ mol}^{-1} \cdot \text{K}^{-2}$) and a vanishing local magnetic moment at the intercalated cobaltocene molecules in the normal state. However, the superconducting properties of the parent lattice do not change significantly within the layers upon the intercalation.

Within the framework of the anisotropic GL theory, it is expected for a single gap anisotropic superconductor that the ratio of the upper critical field $H_{c2\parallel}/H_{c2\perp}$ equals the ratio of $\xi_{\parallel}/\xi_{\perp}$, $\lambda_{\perp}/\lambda_{\parallel}$ and $\kappa_{\parallel}/\kappa_{\perp}$ [1]. The anisotropy factor $\Gamma \approx 3.3$ of 2H-NbSe₂ can be extracted from its H_{c2} - and ξ -ratio. In 2H-NbSe₂, the ξ -ratio is slightly larger than the corresponding λ - (1.6) and κ -ratio (2.2). For the intercalated sample $\text{NbSe}_2\{\text{CoCp}_2\}_{0.26}$ we observe a higher anisotropy factor of about 4.4, which is equal to the ξ ratio, but is significantly smaller than the λ - (7.8) and κ -ratio (5.9). These results therefore suggest that the anisotropic superconducting behavior in $\text{NbSe}_2\{\text{CoCp}_2\}_{0.26}$ cannot be described and modeled within the framework of the anisotropic GL theory involving an anisotropy in the effective masses [1]. This is especially true for a pronounced anisotropic system where the layer distance is of the same order of magnitude as the coherence length [10]. An alternative approach for the description of a layered superconductor based on Josephson-coupled 2D layers leads to a somewhat different expression for $H_{c1\parallel}$ [39]. However, the numerical values for the λ - and κ -ratio for $\text{NbSe}_2\{\text{CoCp}_2\}_{0.26}$ are almost identical to those obtained above.

4.3. Peak effect

As mentioned in section 4.2 the temperature-dependent in-plane resistivity in various magnetic fields shows a reentrant superconducting behavior (see figure 5(b)). This behavior is directly associated with a peak effect which is frequently found in layered type-II superconductors, including the host sample 2H-NbSe₂ (see, for example, [43]). The observed peaks in the resistivity data $\rho(T)$ in figure 5(b) might be a consequence of two competing mechanisms: superconductivity and flux motion controlled resistivity. Therefore, an analysis of the temperature-dependent resistivity could provide a measure of the average vortex velocity. For conventional low temperature superconductors this effect is primarily observed in the regime of the upper critical field $\mu_0 H_{c2}$ and indicates the presence of different superconducting phases arising from a change of flux motion [44]. For example, a highly dense vortex liquid phase

is expected below $\mu_0 H_{c2}$, when the layer separation, d , is of the same order of magnitude as the coherence length ξ [10]. For $\text{NbSe}_2\{\text{CoCp}_2\}_{0.26}$ this criterion is nearly fulfilled when the magnetic field is applied perpendicular to the layers. In that case d becomes compatible in magnitude with $\xi_{\perp}/2$ (see table 1).

In order to deal more precisely with the temperature dependent resistivity in the superconducting phase of $\text{NbSe}_2\{\text{CoCp}_2\}_{0.26}$ we present in figures 7(a) and (b) enlarged plots of $\rho(T)$ near T_c in two selected magnetic fields, 0 T and 10 T, respectively. In a zero magnetic field, $\text{NbSe}_2\{\text{CoCp}_2\}_{0.26}$ exhibits the highest superconducting critical temperature, $T_c^{\text{onset}} = 7.5 \text{ K}$, observed so far in the intercalated or substituted 2H-NbSe₂ samples (see section 4.1). Towards lower temperatures and after the initial superconducting drop, the resistivity shows a pronounced shoulder around 7.4 K, followed again by a steep drop until $\rho(T)$ vanishes on further cooling. This observation hints at two competing mechanisms which control the $\rho(T)$ behavior of the intercalated NbSe₂ phases. In order to identify this additional contribution a single superconducting transition has been modeled by a Boltzmann-type sigmoidal function to fit the experimental data (disregarding the temperature region between 7.2 K and 7.4 K). In figure 7(a) the dashed red line depicts the superconducting transition according to the Boltzmann-type sigmoidal function:

$$\rho_{\text{fit}} = \rho_{\text{high}} - \frac{\rho_{\text{high}}}{1 + e^{(T-T_c)/\Delta T}}, \quad (5)$$

with ρ_{high} being the normal state resistivity at $T = 8 \text{ K}$ and ΔT the slope factor. Here, $T_c = 7.39 \text{ K}$ is calculated from the ρ_{fit} -data (the dashed red line in figure 7(a)) and taken as the temperature, where the resistivity drops by 50% with respect to the value of the normal state resistivity at 8 K. Subtracting the received superconducting contribution from the experimental data results in a peak-like feature (the solid green line in figure 7(a)). From this differential curve two characteristic temperatures are obtained. $T_{p1}(T)$ is defined by the intersection of the Boltzmann curve with the difference curve, and $T_{p2}(T)$ marks the position of the maximum of the extracted peak. With increasing magnetic fields the shoulder shifts to lower temperatures, until it renders into a separate peak, whose height increases with increasing fields (figure 7(b)). In this case, T_{p1} and T_{p2} are marked as the local minimum and maximum of $\rho(T)$, respectively. The results of this investigations are summarized in the H - T -phase diagram for H_{\parallel} in figure 9(a). It should be mentioned that the H - T -phase diagrams of the intercalated sample and the host substance in the highly dense vortex liquid phase are very similar, with exception of the upper critical field area [14].

The presence of a peak effect is also supported by AC-susceptibility measurements. In figures 8(a) and (b) the imaginary and real part of the AC-susceptibility, $\chi_V''(T)$ and $\chi_V'(T)$, are plotted for $\text{NbSe}_2\{\text{CoCp}_2\}_{0.26}$ in an applied magnetic DC-field of 2 T and 3 T perpendicular to the layers. Similar to the resistivity measurements, a pronounced peak effect is determined from the AC-susceptibility data. For $\chi_V'(T)$ a distinct peak develops, again characterized by the two temperatures T_{p1} and T_{p2} , which mark the local minimum

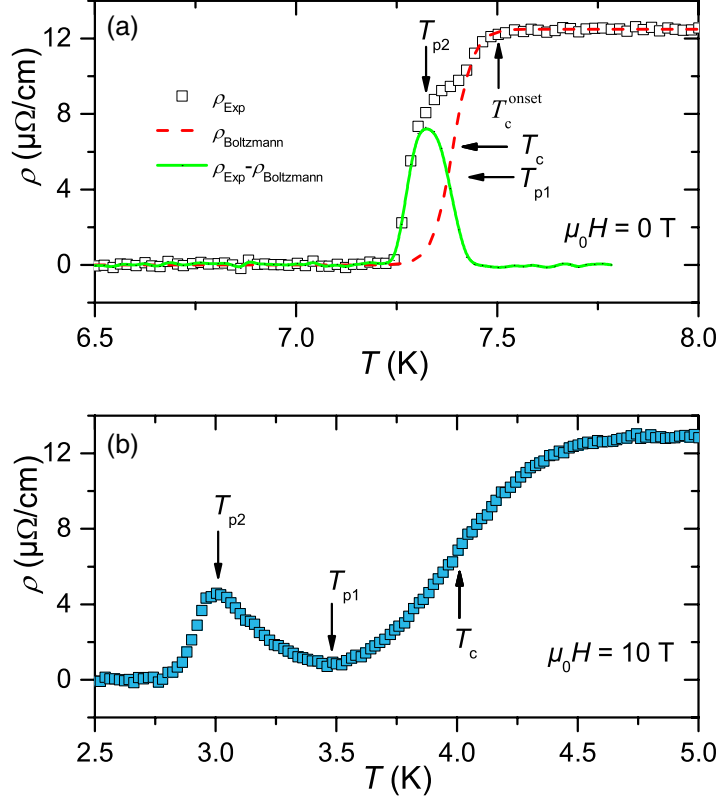


Figure 7. An enlarged presentation of the temperature dependent electrical resistivity in an applied magnetic field of (a) 0 T and b) 10 T perpendicular to the layers. In (a) the red dashed line represents the Boltzmann sigmoidal function adapted to the data, and the green line is the differential plot between the measured data and the adapted curve. For the definitions of the temperatures T_c^{onset} , T_c , T_{p1} and T_{p2} see text.

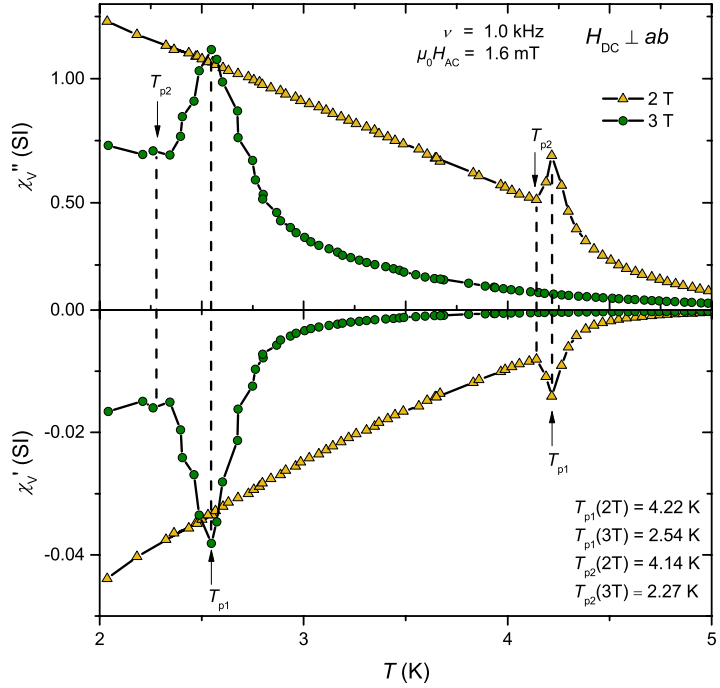


Figure 8. The temperature dependent AC-susceptibility ($\nu = 1$ kHz; $\mu_0 H_{AC} = 1.6$ mT) (a) χ_V'' and (b) χ_V' of $\text{NbSe}_2[\text{CoCp}_2]_{0.26}$ in an applied DC-magnetic field of 2 T and 3 T perpendicular to the layers.

and the local maximum, respectively. However, in the cases of $\chi_V''(T)$ the situation is reversed (see figures 8(a) and (b)). The resulting temperature-dependent characteristic magnetic fields, $\mu_0 H_{p1\perp}(T)$ and $\mu_0 H_{p2\perp}(T)$, are summarized in the

H - T -phase diagram for H_{\perp} in figure 9(b). In the case of $H_{\parallel}(T)$ (figure 9(a)) $\chi_V'(T)$ and $\chi_V''(T)$ could only be analyzed up to 0.6 T. Nevertheless, for this low field region the $H_{\parallel}(T)$ values of the characteristic temperatures, determined from

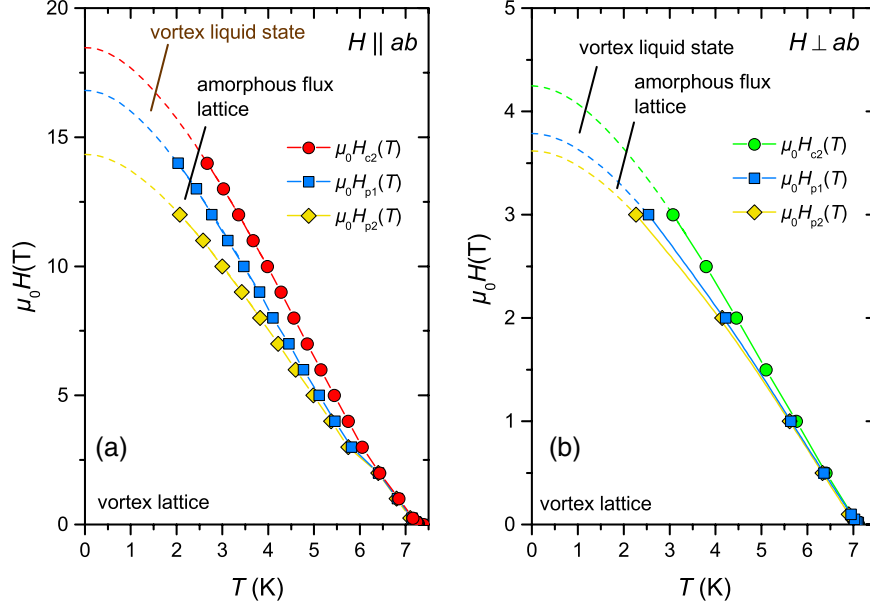


Figure 9. H - T -phase diagram of $\text{NbSe}_2\{\text{CoCp}_2\}_{0.26}$ in an applied magnetic field (a) parallel and (b) perpendicular to the layers. The phase boundaries for the vortex-liquid phase and the amorphous vortex lattice phase are determined in the case of $H \parallel ab$ from the resistivity measurements and for $H \perp ab$ from the AC-susceptibility data.

the susceptibility data, nicely agree with the values from the resistivity measurements [14].

The phase diagrams in both directions (figures 9(a) and (b)) exhibit three different phases in the mixed state which broaden with increasing magnetic fields. Such behavior is also found in 2H-NbSe_2 for H perpendicular to the layers [33, 45]. For the dilute vortex state in low magnetic fields, no phase separation up to 2 T for H_{\parallel} and 0.5 T for H_{\perp} is observed. For the host sample a clear separation occurs in this region, which broadens with decreasing fields [46]. This different behavior in the dilute vortex region may be due to an unusual quantized flux penetration, as discussed in section 4.2.

In weakly pinned type-II superconductors, the vortex assemblage acts more or less as an elastic medium in a random pinning environment which can be activated thermally or driven by disorder. In both cases the shear forces between the single vortices get stronger than the pinning force. Intrinsic pinning centers are most likely in the large gaps between the superconducting layers; a scenario which is also discussed for HTC superconductors [47]. In the latter case, the mixed phase is not homogeneous but consists of different complex vortex phases [43]. In the simplest case the vortex lattice changes from a solid state, where the vortex array is fixed in an ordered Abrikosov- or in a slightly disordered Bragg phase, to an amorphous state (glass phase) and, finally, into a vortex liquid state, where the vortex flux motion is reversible. In comparison to the phase diagram of 2H-NbSe_2 , the region between the $\mu_0 H_{c2}$ and $\mu_0 H_{p1}$ borderlines is related to the liquid state, followed by an amorphous state between the $\mu_0 H_{p1}$ and $\mu_0 H_{p2}$ lines. Due to the complex nature of vortex phases, a vast number of detailed studies have been performed in the case of high T_c as well as low T_c superconductors, see, e.g. [10, 33, 48, 49]. To analyze the complicated vortex phase structure in $\text{NbSe}_2\{\text{CoCp}_2\}_{0.26}$, further investigations are warranted which also consider the subtle pinning behavior of

this type-II superconductor in greater detail, as well as the presence of large van der Waals gaps and intercalated guest molecules which might act as pinning centers.

5. Anisotropy and the specific heat

The unusual temperature dependence of the electronic specific heat ΔC , which is shown in figure 5(a) for the intercalated material $\text{NbSe}_2\{\text{CoCp}_2\}_{0.26}$, is also evidenced by the parent compound 2H-NbSe_2 and thus not controlled by the presence/absence of charge donation by the guest molecules. This feature has, however, raised an intense discussion on the role of the anisotropy of the material on $\Delta C(T)$ sequences. Kobayashi *et al* showed already in 1977 that the almost linear dependence of $\Delta C/T$ on T^2 can be explained by the anisotropy of the layered 2H-NbSe_2 [13]. They assumed an enhancement of the effective electron mass m_{\perp}^* in the out-of-plane direction, as compared to the effective mass m_{\parallel}^* in the planes, as well as a reduction in the superconducting energy gap perpendicular to the plane as an origin of the peculiar $\Delta C(T)$ behavior. The discovery of a similar, almost linear T^2 -dependence of $\Delta C/T$ in the two-gap superconductor MgB_2 [7], however, led to the supposition that in 2H-NbSe_2 the presence of two energy gaps with unequal magnitudes might also be the essential prerequisite for this $\Delta C(T)$ feature. Huang *et al* tested this hypothesis by fitting the specific heat obtained through various anisotropic gap models to their experimental data and compared these results with fits relying on a two-gap model [29, 50]. These authors focused, however, mainly on the comparison of a two-gap model versus a superconducting (single) energy gap model with a six-fold symmetric in-plane anisotropy, which is supposed to reflect the symmetry of the crystal lattice. Their conclusion was that the two energy gap model performs better at describing the experimental data in the case of the selected benchmark systems.

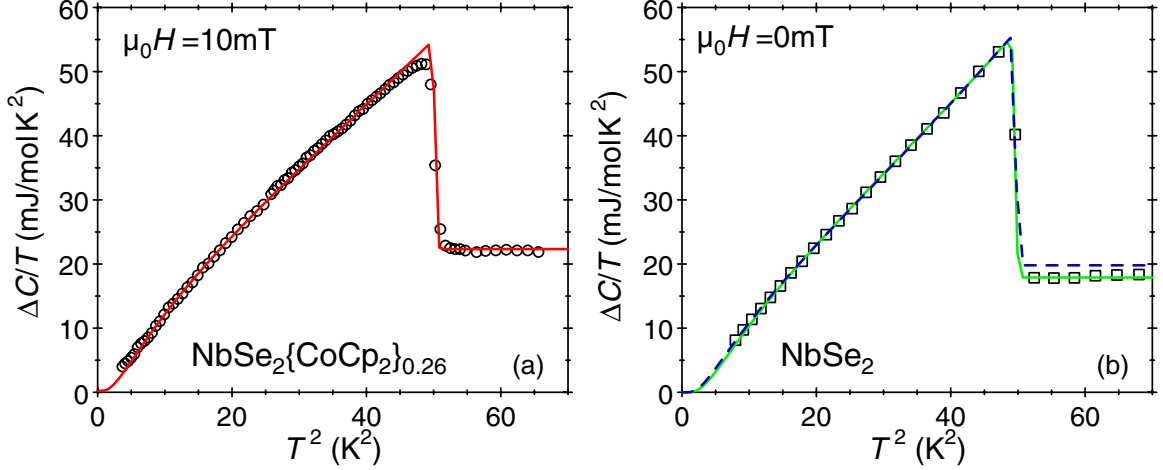


Figure 10. Fits (the solid lines) to the experimental data (the circles and squares) for $\Delta C/T$ as a function of T^2 for (a) the intercalated $\text{NbSe}_2\{\text{CoCp}_2\}_{0.26}$ (data also shown in figures 5(a) and (b)) the parent compound 2H-NbSe₂, respectively. In (a) the ratio $\Delta(T=0)/T_c = 1.76$ is fixed to the BCS value and an anisotropy $\nu = m_{\parallel}^*/m_{\perp}^* = 0.08$ is used. In (b), the ratio $\Delta(T=0)/T_c = 2.09$ is adapted to reproduce the correct value for $\delta C/\gamma T_c$ and an anisotropy $\nu = 0.6$ is used (the solid green line). The dashed line shows $\Delta C/T$ for an isotropic system ($\nu = 1$), where $\Delta(T=0)/T_c = 1.99$ is adapted to reproduce $\Delta C/T$ best below T_c .

Since our benchmark system allows a direct control of the sample's anisotropy factor via intercalation, we repeated the comparison of the performance of these different models to fit the $C(T)$ data in low dimensional superconductors. Our approach follows the ansatz of Kobayashi *et al* [13] and assumes an enhanced effective mass m_{\perp}^* reflecting the system's anisotropy, whereas the gap function Δ is kept constant. The electronic specific heat of the superconducting state is given within the BCS theory [28] as:

$$C = \frac{2N_0}{T} \int \frac{d^2\mathbf{k}}{4\pi} \frac{\partial f_{\mathbf{k}}}{\partial E_{\mathbf{k}}} \left(E_{\mathbf{k}}^2 - \frac{T}{2} \frac{d\Delta^2(T)}{dT} \right), \quad (6)$$

where $f_{\mathbf{k}} = 1/(1 + e^{E_{\mathbf{k}}/k_B T})$ is the Fermi distribution function and $E_{\mathbf{k}} = \sqrt{\epsilon_{\mathbf{k}}^2 + \Delta^2}$ is the quasi-particle energy. The temperature dependence of $\Delta(T)$ is derived from the self-consistency condition $1/V = \int d^2\mathbf{k} (1 - 2f_{\mathbf{k}})/2E_{\mathbf{k}}$, where V is the pairing interaction strength. The value of V is chosen to give the measured critical temperature T_c . The lattice anisotropy enters through the kinetic energy $\epsilon_{\mathbf{k}} = (\hbar^2/2)(\mathbf{k}_{\parallel}^2/m_{\parallel}^* + k_{\perp}^2/m_{\perp}^*)$, where \mathbf{k}_{\parallel} is the in-plane momentum and k_{\perp} the out-of-plane momentum.

In order to find a model which reproduces the $\Delta C/T$ data best, it is important to notice that the ratio $\Delta(T=0)/T_c$ has a fixed value within the BCS theory, which is ≈ 1.76 for an isotropic gap function Δ . Nevertheless, this ratio deviates somewhat from the BCS value in most superconductors, in particular, it is slightly enhanced in 2H-NbSe₂. A consequence of this enhancement is an increased specific heat jump $\delta C/\gamma T_c$, for which the reported values vary somewhat (see table 1). The shape of the calculated curve $\Delta C/T$ depends strongly on the chosen value for the ratio $\Delta(T=0)/T_c$ (see, e.g. [50]), wherefore this ratio is taken as a fitting parameter in [13, 29, 50]. In our measurements on $\text{NbSe}_2\{\text{CoCp}_2\}_{0.26}$, we find that the ratio $\delta C/\gamma T_c \approx 1.43$ is in perfect agreement with the BCS result (figure 10(a)). The non-intercalated 2H-NbSe₂

(figure 10(b)), however, deviates from the BCS result with a ratio $\delta C/\gamma T_c \approx 2.05$.

Because of the good agreement of $\text{NbSe}_2\{\text{CoCp}_2\}_{0.26}$ with the BCS result, we chose as a model ansatz for ΔC the pure BCS model with one isotropic gap and only the one fitting parameter $\nu = m_{\perp}^*/m_{\parallel}^*$. Varying ν does not alter the ratio $\delta C/\gamma T_c$, but changes the curvature of $\Delta C/T$, which makes this model especially suitable for reproducing our measured data. Figure 10(a) presents our data for $\text{NbSe}_2\{\text{CoCp}_2\}_{0.26}$ for $\mu_0 H = 10$ mT (which is almost identical to $\mu_0 H = 0$), and the calculated results (the solid red line) for $\nu = 0.08$. While the low- and middle-temperature regime is remarkably well reproduced by our model, the measured $\Delta C/T$ is somewhat reduced close to T_c . This reduction, which is also reported in [51], is not captured in the BCS description but is likely caused by a regime of enhanced superconducting fluctuations around T_c , as can be expected in dimensionally reduced systems.

Figure 10(b) presents our measured results for the parent compound 2H-NbSe₂ in a zero magnetic field. Because of the enhanced ratio $\Delta C/\gamma T_c$, this result is only reproducible if $\delta C/\gamma T_c$ is used as a fitting parameter as well. The solid green line shows the calculated result with anisotropy $\nu = 0.6$ and $\Delta(T=0)/T_c = 2.09$. Within this model, the data shown in [13, 29, 30] are also well reproducible. Remarkably, $\Delta C/T$ is also ideally reproduced below T_c for an isotropic model ($\nu = 1$) if $\Delta(T=0)/T_c$ is adapted only for $T < T_c$, ignoring the height of the discontinuity in $\Delta C/T$. This is illustrated by the dashed line in figure 10(b). This means that if one allows for the presence of an additional mechanism (which is not captured in equation (6)) influencing $\delta C/\gamma T_c$, then an isotropic single-gap model with an isotropic Fermi surface is sufficient to explain the $\Delta C/T$ data.

These observations allow the conclusion that both the intercalated and the non-intercalated material exhibit an $m_{\perp}^*/m_{\parallel}^*$ anisotropy, but while the non-intercalated material harbors an essentially three-dimensional electronic state ($\nu = 0.6$), the single NbSe₂ layers are almost decoupled in the

intercalated material ($\nu = 0.08$). Nevertheless, both materials exhibit a three-dimensional superconducting state, although the anisotropy is increased through intercalation (see table 1). A possibly anisotropic gap, as well as the presence of a second gap, may still add to the characteristic, almost linear $\Delta C/T(T^2)$ behavior of NbSe₂. In view of the generally good agreement of our measurements with the predictions from the BCS theory and their reproducibility by a model ansatz using a single anisotropic Fermi surface, we believe, however, that the main effect on $\Delta C/T$ originates from the anisotropy in the effective masses m_{\parallel}^* and m_{\perp}^* .

6. Conclusion

The layered superconductor 2H-NbSe₂ has been intercalated with the organometallic donor molecule cobaltocene to yield single-phase and crystalline NbSe₂{CoCp₂}_{0.26} samples. A small increase in the superconducting transition temperature $T_c^{\text{onset}} = 7.5$ K is observed upon intercalation, which represents the highest value of the intercalated or substituted 2H-NbSe₂ species reported so far. Structural characterization confirms that the lattice spacing perpendicular to the superconducting layers increases significantly upon intercalation and is twice as large as for the host lattice. This expansion alters the superconducting properties within the layers only marginally, but has a strong influence on the nature of the superconductivity perpendicular to the NbSe₂ layers. The virtually decoupled arrangement of the NbSe₂ layers in the intercalate increases the anisotropy factor of $\Gamma = H_{c2\parallel}/H_{c2\perp} = 4.4$ by 34% relative to native 2H-NbSe₂. This observation is paralleled by an increase in the upper critical field $\mu_0 H_{c2\parallel} = 18.5$ T versus the parent compound 2H-NbSe₂ (14.1 T). The fact that Γ calculated from the ξ ratio differs strongly from the corresponding values derived from the λ - and κ -ratio provides another hint that the anisotropic GL theory fails to describe the incidence of superconductivity in NbSe₂{CoCp₂}_{0.26}. In addition, NbSe₂{CoCp₂}_{0.26}, as well as 2H-SnSe₂, exhibits a reentrant peak effect in the magnetic fields parallel and perpendicular to the layers. This observation suggests the presence of complex vortex phases in the mixed state as a second contribution to the superconducting scenario.

Although the intercalated dichalcogenide NbSe₂{CoCp₂}_{0.26} exhibits a strongly enhanced anisotropy, surprisingly we found that the ratio $\delta C/\gamma T_c = 1.43$ is in good agreement with the prediction from the BCS theory. Based on the $\Delta C/T$ data fits, the superconducting scenario in both dichalcogenides, NbSe₂{CoCp₂}_{0.26} and the parent compound 2H-NbSe₂, can be described by a one-gap BCS model with an anisotropic Fermi surface in contrast to earlier findings in the literature, which favored a two-gap scenario.

Acknowledgments

This work was supported by the Deutsche Forschungsgemeinschaft (project number SCHE487/12-1 and TRR 80).

References

[1] Klemm R A 2012 *Layered Superconductors* vol 1 (Oxford: Oxford University Press) chapter 8

- [2] Scherer W *et al* 2010 *Angew. Chem. Int. Edn* **49** 1578
- [3] Scheidt E-W, Hauf C, Reiner F, Eickerling G and Scherer W 2011 *J. Phys.: Conf. Ser.* **273** 012083
- [4] Nagamatsu J, Nakagawa N, Muranaka T, Zenitani Y and Akimitsu J 2001 *Nature* **410** 63
- [5] Scheidt, E-W, Hathwar V R, Schmitz D, Dunbar A, Scherer W, Mayr F, Tsurkan V, Deisenhofer J and Loidl A 2012 *Eur. Phys. J. B* **85** 279
- [6] Revolinsky E, Spiering G A and Beerntsen D J 1965 *J. Phys. Chem. Solids* **26** 1029
- [7] Bouquet F, Wang Y, Fisher R A, Hinks D G, Jorgensen J D, Junod A and Phillips N E 2001 *Europhys. Lett.* **56** 856
- [8] Zehetmayer M and Weber H W 2010 *Phys. Rev. B* **82** 014524
- [9] Meyer S F, Howard R E, Stewart G R, Acrivos J V and Geballe T H 1975 *J. Chem. Phys.* **62** 4411
- [10] Banerjee S S *et al* 1998 *Europhys. Lett.* **44** 91
- [11] Harper J M E, Geballe T H and DiSalvo F J 1977 *Phys. Rev. B* **15** 2943
- [12] Rossmagel K, Seifarth O, Kipp L, Skibowski M, Voß D, Krüger P, Mazur A and Pollmann J 2001 *Phys. Rev. B* **64** 235119
- [13] Kobayashi N, Noto K and Muto Y 1977 *J. Low Temp. Phys.* **27** 217
- [14] Herzinger M 2013 *Interkalationsverbindungen von NbSe₂ und SnSe₂: Modellsysteme für niederdimensionale Supraleiter* *Dissertation* Augsburg University
- [15] Petricek V, Dušek M and Palatinus L 2014 *Z. Kristallogr. Cryst. Mater.* **229** 345
- [16] Dines M B 1975 *Science* **188** 1210
- [17] Presnitz M 2014 *Untersuchungen an Materialien mit niederdimensionalen Eigenschaften* *Dissertation*, Augsburg University
- [18] Toyota N, Nakatsuji H, Noto K, Hoshi A, Kobayashi N, Muto Y and Onodera Y 1976 *J. Low Temp. Phys.* **25** 485
- [19] Ikebe M, Katagiri M, Noto K and Muto Y 1980 *Physica B + C* **99** 209
- [20] Dalrymple B J and Prober D E 1984 *J. Low Temp. Phys.* **56** 545
- [21] Naik I and Rastogi A K 2011 *Pramana* **76** 957
- [22] Presnitz M, Herzinger M, Scheidt E-W, Scherer W, Baenitz M and Marz M 2012 *Meas. Sci. Technol.* **23** 085002
- [23] Hillenius S J and Coleman R V 1979 *Phys. Rev. B* **20** 4569
- [24] Iavarone M, DiCapua R, Karapetrov G, Koshelev A E, Rosenmann D, Claus H, Malliakas C D, Kanatzidis M G, Nishizaki T and Kobayashi N 2008 *Phys. Rev. B* **78** 174518
- [25] Scheidt E-W, Hucho C, Lüders K and Müller M 1989 *Solid State Commun.* **71** 505
- [26] Denhoff M W and Gygax S 1982 *Phys. Rev. B* **25** 4479
- [27] Tinkham M 1996 *Introduction to Superconductivity* 2nd edn (New York: McGraw-Hill)
- [28] Bardeen J, Cooper L N and Schrieffer J R 1957 *Phys. Rev.* **108** 1175
- [29] Huang C L, Lin J, Chang Y T, Sun C P, Shen H Y, Chou C C, Berger H, Lee T K and Yang H D 2007 *Phys. Rev. B* **76** 212504
- [30] Jing Y, Lei S, Yue W, Zhi-Li X and Hai-Hu W 2008 *Chin. Phys. B* **17** 2229
- [31] Lin J Y, Hsieh Y S, Chareev D A, Vasiliev A N, Parsons Y and Yang H D 2011 *Phys. Rev. B* **84** 220507
- [32] Lyard L *et al* 2002 *Phys. Rev. B* **66** 180502
- [33] Tomy C V, Pal D, Banerjee S S, Ramakrishnan S, Grover A K, Bhattacharya S, Higgins M J, Balakrishnan B and Mck Paul D 2002 *Pramana* **58** 925
- [34] Edwards J and Frindt R F 1971 *J. Phys. Chem. Solids* **32** 2217
- [35] Werthamer N R, Helfand E and Hohenberg P C 1966 *Phys. Rev.* **147** 295
- [36] Klemm R A, Luther A and Beasley M R 1975 *Phys. Rev.* **12** 877

- [37] Angst M, Puzniak R, Wisniewski A, Jun J, Kazakov S M, Karpinski J, Roos J and Keller H 2002 *Phys. Rev. Lett.* **88** 167004
- [38] Muto Y, Toyota N, Noto K and Hoshi A 1973 *Phys. Lett. A* **45** 99
- [39] Ginzburg V L and Kirzhnits D A 1986 *High Temperature Superconductivity* (New York: Consultants Bureau)
- [40] de Trey P, Gygax S and Jan J-P 1973 *J. Low Temp. Phys.* **11** 421
- [41] Sanchez D, Junod A, Muller J, Berger H and Lévy F 1995 *Physica B* **204** 167
- [42] Soto F, Berger H, Cabo L, Carballeira C, Mosqueira J, Pavuna D and Vidal F 2007 *Phys. Rev. B* **75** 094509
- [43] Zhu X D, Lu J C, Sun Y P, Pi L, Qu Z, Ling L S, Yang Z R and Zhang Y H 2010 *J. Phys.: Condens. Matter* **22** 505704
- [44] Mikitik G P and Brandt E H 2001 *Phys. Rev. B* **64** 184514
- [45] Ghosh K *et al* 1996 *Phys. Rev. Lett.* **76** 4600
- [46] Ramakrishnan S *et al* 1996 *Czech. J. Phys.* **46** 3105
- [47] Tachiki M and Takahashi S 1989 *Solid State Commun.* **70** 291
- [48] Thakur A D, Chandrasekhar Rao T V, Uji S, Trrashima T, Higgins M J, Ramakrishnan S and Grover A K 2006 *J. Phys. Soc. Japan* **75** 074718
- [49] Thakur A D, Banerjee S S, Higgins M J, Ramakrishnan S and Grover A K 2006 *Pramana J. Phys.* **66** 159
- [50] Huang C L, Lin J-Y, Sun C P, Lee T K, Kim J D, Choi E M, Lee S I and Yang H D 2006 *Phys. Rev. B* **73** 012502
- [51] Kačmarčík J, Pribulová Z, Marcenat C, Klein T, Podière P, Cario L and Samuely P 2010 *Phys. Rev. B* **82** 014518